IEEE Access
Multidisciplinary | Rapid Review | Open Access Journal

Received September 22, 2018, accepted October 9, 2018, date of publication October 25, 2018,
date of current version November 30, 2018.

Digital Object Identifier 10.1109/ACCESS.2018.2877958

Localizing Noncooperative Receiver Through Full-Duplex Amplify-and-Forward Relay

CHUANXUE JIN[1], (Member, IEEE), BO CHANG[1], (Student Member, IEEE), GUODONG ZHAO[2], (Senior Member, IEEE), ZHI CHEN[1], (Senior Member, IEEE), AND YUAN SHEN[3], (Member, IEEE)

[1]National Key Laboratory of Science and Technology on Communications, University of Electronic Science and Technology of China, Chengdu 611731, China
[2]School of Engineering, University of Glasgow, Glasgow G12 8LT, U.K.
[3]Department of Electronic Engineering, Tsinghua University, Beijing 100084, China

Corresponding author: Guodong Zhao (guodong.zhao@glasgow.ac.uk)

This work was supported in part by the National Natural Science Foundation of China under Grant 61601094, in part by the National Natural Science Foundation of China under Grant 61631004, and in part by the Important National Science and Technology Specific Projects of China under Grant 2018ZX03001001.

ABSTRACT Localizing noncooperative *transmitter* (Tx) and *receiver* (Rx) that belong to another system is important in many scenarios, e.g., interference management in cognitive radio systems and user behavior learning in ad hoc wireless networks. However, obtaining the locations of these nodes in particular in *frequency-division duplex* systems is challenging, since the localization network usually does not know the spectrum that the Rx uses for backward transmission. In this paper, we propose to use the full-duplex relay technique to localize a noncooperative Rx, which does not require the knowledge of the Rx's backward transmission spectrum. In the proposed method, localization sensors alternatively act as a full-duplex *amplify-and-forward* relay to trigger the power control of the Tx–Rx link. Then, by detecting the power adjustment of the Tx, each localization sensor can estimate the *time difference of arrival* between the direct and relay signals. Finally, the Rx location can be calculated from triangulation. Simulation results show that the proposed method can effectively localize the Rx, which validates its potential for receiver-aware applications and services.

INDEX TERMS Estimation, full-duplex relay, localization, receiver.

I. INTRODUCTION

A. BACKGROUND

Even though wireless localization technique has been extensively studied in the past decades [1]– [12], there is still no effective method for the applications requiring the location of the noncooperative *receiver* (Rx), i.e., the receiver that belongs to another system. For example, in *frequency duplex division* (FDD) cognitive radio networks, the location of primary Rx is critical for underlay spectrum sharing. With the help of the primary Rx location, the cognitive user is able to dynamically adjust transmission power and maximize the cognitive throughput [13]. For another example, in Ad Hoc networks, localizing noncooperative Rx is critical to obtain the association relationship of a group of users, i.e., which user serves which user. As shown in Fig. 1, there are three pairs of users communicating in the FDD mode and occupying six frequency bands. Using existing localization methods, the localization sensors, denoted as $A_1, A_2, ..., A_6$ in the figure, can track down the origin of the wireless signal in each band, and obtain the locations of the six users. But, they do not know the association relationship among them. Therefore, to obtain the association relationship and learn the behavior of these users, the localization sensors need to be capable of localizing Rx for each *transmitter* (Tx).

In practice, localizing noncooperative Rx is difficult in particular in FDD systems. This is because localization sensors usually do not know the spectrum that the Rx uses for backward transmission. As a result, existing localization methods [1]– [12] that track down the origin of wireless signal cannot localize noncooperative Rx.

B. RELATED WORKS

To the best of our knowledge, there are few studies addressing the problem of noncooperative Rx localization. The only

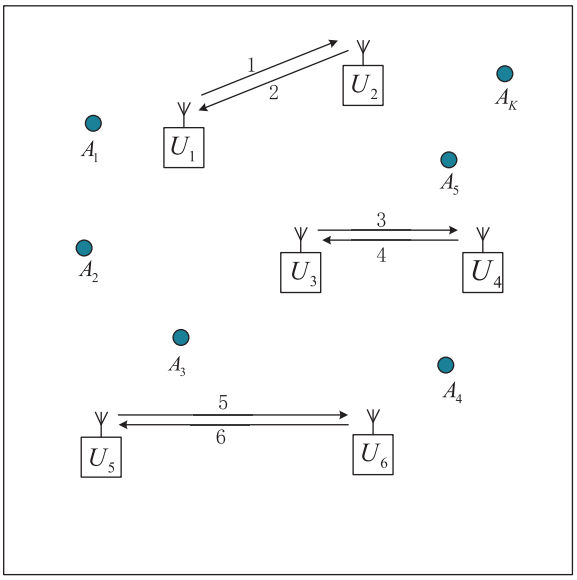

FIGURE 1. Illustration of the association relationship in a FDD Ad Hoc Network.

related one is the advanced sensing technique [14] that has been recently developed in cognitive radio systems. The goal is to detect and estimate the information related to non-cooperative primary Rx under the situation that cognitive user does not know the transmitted signal from primary Rx. In principle, the advanced sensing treats the interference from a cognitive Tx to a primary Rx as a probing signal. Then, the cognitive user can adjust its transmission power and artificially trigger the link adaption of the primary communication [15], e.g., the *power control* (PC), *automatic modulation and coding* (AMC), and *automatic retransmission request* (ARQ). By observing the response of the primary signal that comes from the primary Tx, the cognitive user is able to obtain the required information related to the primary Rx. It has been shown in [16]– [20] that the cognitive user can effectively detect the nearby primary Rx and further estimate the wireless channel gain between the cognitive Tx and primary Rx. In [21] and [22], the full-duplex relay technique has recently been introduced into the advanced sensing, which can significantly reduce the interference to the primary system caused by the probing signal.

C. PROPOSED SOLUTION

Motivated by the recent progress on advanced sensing technique, we propose a new method to use the full-duplex relay technique to localize the noncooperative Rx. In our method, we have a Tx-Rx link from a system. Some localization sensors from another system intend to localize the Rx. We assume that the localization sensors know the locations of the Tx and their own. The way to localize the Rx is to use the knowledge that the Rx will only jointly process the received signals if the *time-difference-of-arrival* (TDOA) of signals arrive at the Rx is less than a time window $T_{\max}$. Thus, we use each localization sensors (one at a time) as a full-duplex *amplified-and-forward* (AF) relay, and then the Rx will receive both Tx and relay signals. Next, the localization sensor delays the relay signal until it is received with a TDOA that is larger than $T_{\max}$. When this happens, the power control of the Tx-Rx link will see a drop in signal power at the Rx since the relay signal is now treated as interference. As a response, the power control will boost up the Tx transmission power and the localization sensor acting as a relay will observe this. Knowing the delay that the localization sensor imposed at this time, each localization sensor can compute the TDOA and then localize the Rx from triangulation.

We need to note that in [23] and [24], we have obtained two methods using TDOA to calculate the location of the noncooperative Rx. In [23], both the angle-of-arrival (AOA) and TDOA were adopted to obtain the Rx location. In [24], only TDOA was adopted in the calculation of the Rx location. However, none of them discussed the performance of the proposed methods and their effect on the overall systems. In addition, the design of the localization methods was not clearly described in these two papers. In the following, we summarize the main contributions of this paper:

- we propose a new method to use the full-duplex relay technique to localize the noncooperative Rx, which does not require the localization sensors to measure the wireless signal from the Rx;
- we propose a delay-relay algorithm to allow each localization sensor to autonomously obtain the TDOA between the direct and relay paths, and calculate the Rx location;
- we investigate the impacts of the proposed localization method on the Tx-Rx link, which shows the feasibility of the proposed method.

D. PAPER STRUCTURE

The rest of this paper is organized as follows. In Section II, we provide the system model, the main assumptions, and the signal model. In Section III, we propose our Rx localization method that uses the full-duplex relay technique. In Section IV, we analyze the power adjustment of the Tx, which indicates the impacts of our method on the Tx-Rx link. In Section V, we demonstrate the performance of the proposed approach. Finally, Section VI concludes the paper and discusses the potential research directions.

II. SYSTEM MODEL

A. SYSTEM MODEL AND MAIN ASSUMPTIONS

Fig. 2 provides the system model of this paper. As shown in Fig. 2(a), the Tx at $(0, 0)$ serves a Rx at (x, y) via a certain spectrum. The geographic distance between the Tx and the Rx is d_0 and the radius of the Tx's coverage is R. In the meantime, K localization sensors from another system, located at (x_k, y_k) for $1 \leq k \leq K$, intend to obtain the location of the Rx. They know the location of the Tx and their own. They can alternatively conduct the full-duplex AF relaying and the corresponding timing diagram is shown in Fig. 2(b). Here, we consider the block fading channel,

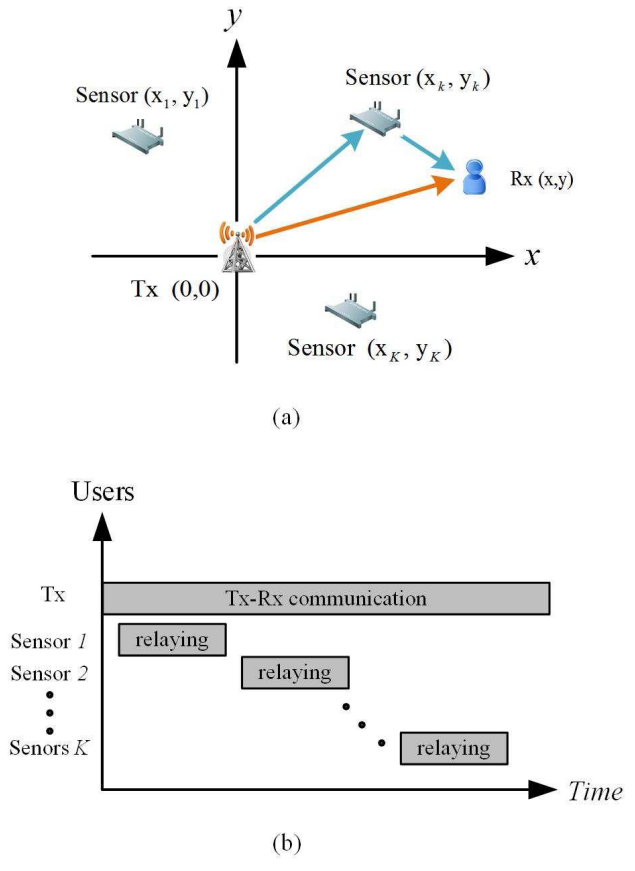

FIGURE 2. System model: (a) Geographic model of different users; (b) Timing diagram of different users.

where the sample period and the block period are denoted as T_s and T_b, respectively. Next, we make the following set of assumptions to localize the Rx.

- The Tx-Rx link uses *close-loop power control* (CLPC)[1] to maintain the target average *signal-to-noise ratio* (SNR) or *signal-to-interference-plus-noise ratio* (SINR) of the Rx, both denoted as $\bar{\gamma}_T$;
- The localization sensors do not know the spectrum that the Rx uses for CLPC feedback[2];
- The Rx only jointly processes the signals that arrive at the Rx within a TDOA of $T_{\max}$.

Thus, if the two signals[3] arrive at the Rx with a TDOA less than or equal to $T_{\max}$, i.e., $\tau_k \leq T_{\max}$, both produce the signal power, which is shown in Fig. 3(a). If the two signals arrive at the Rx with a TDOA larger than $T_{\max}$, i.e., $\tau_k > T_{\max}$,

[1]Here, we consider the perfect CLPC, which means that the Tx can adjust the transmission power to the required value without time delay and quantization. The impact of the CLPC imperfection is beyond the scope of this paper

[2]This is because in FDD systems, the wireless channel that carries the CLPC feedback changes frequently due to dynamic channel allocation. Thus, it is very hard for the localization sensors to obtain the channel allocation information that belongs to another system

[3]Since this is the first trail study on noncooperative Rx localization, we use two path model to develop our idea.

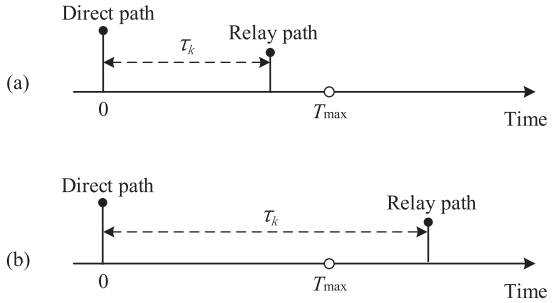

FIGURE 3. The difference of the propagation delays between the direct and relay paths arriving at the Rx: (a) $\tau_k \leq T_{\max}$; (b) $\tau_k < T_{\max}$.

the main path will produce the signal power, and the other will be considered as interference or noise, which is shown in Fig. 3(b).

B. SIGNAL MODEL

In the following, we take one of the localization sensors as an example to introduce signal models before and during conducting the full-duplex AF relaying.

Denote $h_0(j)$ and g_0 as the small-scale fading and large-scale attenuation coefficients for the Tx-Rx link, where $1 \leq j \leq N$ is the index of N blocks, $\mathbb{E}[|h_0(j)|^2] = 1$, and $\mathbb{E}[\cdot]$ represents the expectation operator. We further denote $x(i,j)$ as the transmitted signal from the Tx, and $\mathbb{E}[|x(i,j)|^2] = 1$, where $1 \leq i \leq M$ is the index of M samples in each block. If the transmission power of the Tx, denoted as p_0, is determined by the CLPC, the target average SNR of the Rx can be satisfied, i.e.,

$$\bar{\gamma}_T = \mathbb{E}\left[\frac{|h_0(j)\sqrt{g_0 p_0}x(i,j)|^2}{\sigma^2}\right] = \frac{p_0 g_0}{\sigma^2}, \tag{1}$$

where σ^2 is the variance of the *additive white Gaussian noise* (AWGN) at the Rx.

Denote $h_1(j)$ and g_1 as the small-scale fading and large-scale attenuation coefficients for the Tx-Sensor link, where $\mathbb{E}[|h_1(j)|^2] = 1$. Then the average SNR at the sensor becomes

$$\bar{\gamma}_S = \frac{\mathbb{E}[|h_1(j)\sqrt{g_1 p_0}x(i,j)|^2]}{\sigma^2} = \frac{p_0 g_1 \mathbb{E}[|h_1(j)|^2]}{\sigma^2} = \frac{p_0 g_1}{\sigma^2}, \tag{2}$$

where the sensor and Rx have the same AWGN variance σ^2.

When the sensor conducts the full-duplex AF relaying with the amplitude gain G, its transmitted signal becomes

$$x_S(i,j) = G y_S(i,j), \tag{3}$$

where $y_S(i,j) = h_1(j)\sqrt{g_1 p_0}x(i,j) + n_1(i,j)$ is the received signal at the sensor, and $n_1(i,j)$ is the AWGN at the sensor with mean zero and variance σ^2. Here, we ignore the signal processing delay between reception and transmission since the full-duplex AF relaying is usually implemented through RF circuits with extremely short time delay [25] [26].

We denote $h_2(j)$ and g_2 as the small-scale fading and large-scale attenuation coefficients for the Sensor-Rx link, where $\mathbb{E}[|h_2(j)|^2] = 1$. Then the received signal at the Rx has two

components: the direct signal from the Tx and the relay signal from the sensor. Since they travel through different paths and arrive at the Rx at different time, there is a TDOA between them. Let $\tau = mT_s + nT_b$ as the TDOA, where m and n are the numbers of the sample period T_s and block period T_b, respectively, then the received signal at the Rx can be expressed as

$$\begin{aligned} y'(i,j) = & \underbrace{h_0(j)\sqrt{g_0 p_0}x(i,j)}_{S_d(\text{Direct signal})} \\ & + \underbrace{Gh_2(j)\sqrt{g_2}h_1(j)\sqrt{g_1 p_0}x(i-m,j-n)}_{S_r(\text{Relay signal})} \\ & + \underbrace{Gh_2(j)\sqrt{g_2}n_1(i,j) + n_0(i,j)}_{N(\text{Noise})}, \end{aligned} \tag{4}$$

where $n_0(i,j)$ is the AWGN at the relay with mean zero and variance σ^2.

Here, we do not consider the self-interference caused by the full-duplex relaying because this paper focuses on proposing our new localization idea and demonstrating its feasibility. In fact, the self-interference suppression technique has been extensively studied in full-duplex systems, e.g., [27]. Therefore, we do not design the self-interference algorithm. Instead, we will evaluate the performance loss caused by the imperfect *self-interference suppression* in the simulation part.

III. RELAY-ASSISTED LOCALIZATION METHOD

Localizing the noncooperative Rx is challenging because the localization sensors cannot directly measure the wireless signal from the Rx. To solve the problem, our idea is to let the localization sensors proactively probe the Tx-Rx link using the full-duplex AF relay technique. Then the Tx will automatically adjust the transmission power to maintain the constant signal power at the Rx. By observing the power adjustment of the Tx, the sensors are able to estimate the Rx location.

In the following, we first introduce the proposed Rx localization method. Then, we develop our delay-relay algorithm to estimate the TDOA between the direct and relay paths, which is used to calculate the Rx location. In the next section, we will further analyze the power adjustment of the Tx caused by the proposed localization method. The purpose is to show the proposed method causes minor impacts on the Tx-Rx communication link.

A. PROPOSED RX LOCALIZATION METHOD

The proposed localization method consists of the following steps:

1) *Full-Duplex AF Relaying*: The localization sensor k receives the signal from the Tx, adds a controllable time delay, and then forwards it to the Rx. This artificially creates a relay path between the Tx and Rx. Then we obtain the following equation indicating the distance difference between the two paths, i.e.,

$$\begin{aligned} \Delta d = & \underbrace{\sqrt{x_k^2+y_k^2}}_{\text{Tx-Sensor distance}} + \underbrace{\sqrt{(x-x_k)^2+(y-y_k)^2}}_{\text{Sensor-Rx distance}} \\ & - \underbrace{\sqrt{x^2+y^2}}_{\text{Tx-Rx distance}} = \tau_k \cdot C, \end{aligned} \tag{5}$$

where $C = 3 \times 10^8$ m/s is a constant.

2) *TDOA Estimation*: The localization sensor uses the delay-relay algorithm to estimate the TDOA, which will be further discussed in Section III-B. In the algorithm, the sensor that is relaying the Tx signal artificially delays the relay signal until the TDOA, i.e., τ_k, exceeds the time window $T_{\max}$. When this happens, the sensor detects the power growth of the Tx signal and marks the added time delay as λ_k^*. Then we obtain the following equation

$$\tau_k + \lambda_k^* = T_{\max}. \tag{6}$$

3) *Localization Calculation*: Repeat Steps 1) and 2) by alternatively using K localization sensors, one at a time, where $k = 1, 2, \ldots K$ and $K \geq 3$. Then we obtain K equations as in (5) and also K equations as in (6). Substituting τ_k into (5), we have the following equation array

$$\begin{aligned} & \sqrt{x_k^2+y_k^2} + \sqrt{(x-x_k)^2+(y-y_k)^2} - \sqrt{x^2+y^2} \\ & \quad = C(T_{\max} - \lambda_k^*), \quad \text{for } k = 1, 2, \ldots, K. \end{aligned} \tag{7}$$

By solving the above equation array, we can obtain the location of the Rx (x, y)[4].

B. TDOA ESTIMATION ALGORITHM

In this subsection, we further discuss the TDOA estimation algorithm in our localization method. Here, the TDOA estimation problem is different from the conventional one. Conventionally, the TDOA refers to the time difference of propagation delays that a wireless signal arrives at multiple localization sensors. By measuring the signal and comparing the measurements, the sensors can directly calculate the TDOA. In contrast, the TDOA in this paper refers to the time difference of propagation delays between the direct and relay paths arriving at the Rx. Then, it is hard for the sensors to directly measure the two paths, which raises the main difficult in TDOA estimation.

To solve the problem, we propose a delay-relay algorithm to obtain the TDOA indirectly. Here, we exploit the feature that the Rx only combines the received signals within a time window $T_{\max}$. Any signal that is outside the time window will be treated as interference or noise. Therefore, when the sensor is conducting the relaying, it can artificially delay the relay

[4]Here, the time window $T_{\max}$ is also treated as an unknown variable and can be obtained when we calculate the equation array. Since there are many methods can be used to solve the equation array (7), we do not provide the detailed algorithm here.

signal until the overall TDOA (including the original TDOA τ_k as well as the added time delay λ) larger than the time window $T_{\max}$. When this happens, the Tx will automatically boost up the transmission power. By detecting the power adjustment, the sensor can obtain the value of λ_k^* in (7) and then has the TDOA $\tau_k = T_{\max} - \lambda^*$, where $T_{\max}$ is a constant. Therefore, the key to estimate the TDOA is to detect the power adjustment of the Tx.

In order to detect the power adjustment of the Tx and further estimate the TDOA, we first find a test statistic and then observe its *cumulative distribution function* (CDF). Based on that, we can choose a threshold to detect the power adjustment.

1) FIND THE TEST STATISTIC

Denote ϵ as the increasing step of the added time delay, then the added time delay becomes $\lambda_k = l\epsilon \geq 0$, where $l = 1, 2, ...$ Based on this, we treat the SNR difference at the sensor k, i.e., $\Delta\bar{\gamma}_k' = \bar{\gamma}_l' - \bar{\gamma}_{l-1}'$, as the test statistic, where $\bar{\gamma}_l'$ and $\bar{\gamma}_{l-1}'$ represent the sensor k measured SNRs from the Tx signal before and after adding the time delay ϵ, respectively.

2) ILLUSTRATE THE CDF OF THE TEST STATISTIC

Next, we discuss the relationship between the overall TDOA $\tau_k + \lambda_k$ and the corresponding SNR variation $\Delta\bar{\gamma}_k'$. To simplify the discussion, we let $A = \tau_k + (l-1)\epsilon$ and $B = \tau_k + l\epsilon$ as the overall TDOAs before and after adding the small time delay ϵ. Then, we intuitively have the following relationship:

- If $A < T_{\max}$ and $B < T_{\max}$, the measured SNR does not change too much, i.e., $\Delta\bar{\gamma}_k'$ is small. This is because both $\bar{\gamma}_{l-1}'$ and $\bar{\gamma}_l'$ are observed under $\tau_k + \lambda_k \leq T_{\max}$.
- If $A < T_{\max}$ and $B > T_{\max}$, the measured SNR changes dramatically, i.e., $\Delta\bar{\gamma}_k'$ is large. This is because $\bar{\gamma}_{l-1}'$ is observed under $\tau_k + \lambda_k \leq T_{\max}$, while $\bar{\gamma}_l'$ is observed under $\tau_k + \lambda_k > T_{\max}$.
- If $A > T_{\max}$ and $B > T_{\max}$, the measured SNR again does not change too much, i.e., $\Delta\bar{\gamma}_k'$ is small. This is because both $\bar{\gamma}_{l-1}'$ and $\bar{\gamma}_l'$ are observed under $\tau_k + \lambda_k > T_{\max}$.

Since it is very difficult to obtain the close-form CDF expression of the test statistic $\Delta\bar{\gamma}_k'$, we conduct simulation and provide Fig. 4 to show its CDF curve. Here, the parameter settings come from Section V, which gives us the good localization performance. In particular, the amplitude gain of the relay is $G = 50$ dB. From the figure, when the overall TDOA is small, i.e., $A < T_{\max}$ and $B < T_{\max}$, the SNR variation is small. When the overall TDOA exceeds the maximum allowable TDOA, i.e., $A < T_{\max}$ and $B > T_{\max}$, the SNR variation becomes large. When the overall TDOA is large enough, $A > T_{\max}$ and $B > T_{\max}$, the SNR variation becomes small again. Therefore, the sensor can use the following detector to identify the case that the overall TDOA reaches the maximum allowable TDOA, i.e.,

$$\begin{cases} \tau_k + \lambda_k^* = T_{\max}, & \Delta\bar{\gamma}' \geq \eta, \\ \tau_k + \lambda_k^* \neq T_{\max}, & \Delta\bar{\gamma}' < \eta, \end{cases} \tag{8}$$

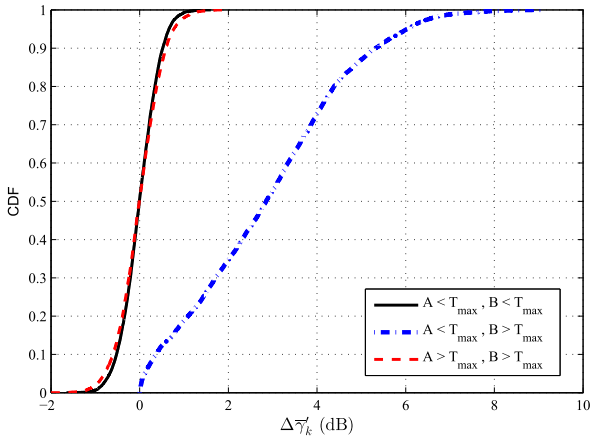

FIGURE 4. The CDF of the SNR variation at each localization sensor.

where η is the detection threshold that will be chosen in Section V.

IV. ANALYSIS OF THE POWER ADJUSTMENT OF THE TX

In this section, we will analyze the power adjustment of the Tx caused by the proposed localization method. This is because our method requires each localization sensor to delay the relay signal until the direct and relay signal are too far apart to be combined at the Rx. When this happens, the relay signal causes interference to the Tx-Rx link, which further triggers CLPC to adjust the transmission power of the Tx. Thus, by analyzing the power adjustment of the Tx, we know how much interference the proposed method introduces.

Specifically, we define $\Delta p_{[dB]} = p_{1[dB]} - p_{0[dB]}$ as the power adjustment of the Tx, where p_0 and p_1 are the Tx transmission powers before and during the relaying, both in dB unit. Let Ω be a threshold of the power adjustment that the Tx is able to tolerant. Then, the interference occurs when the power adjustment of the Tx $\Delta p_{[dB]}$ is larger than the threshold Ω, i.e., $\Delta p_{[dB]} > \Omega$.

In the following, we first use two subsections to discuss the Tx power adjustment and obtain its close-form CDF expression. In the third subsection, we will show how much interference the proposed method introduces.

A. TX POWER ADJUSTMENT

Since the Tx power adjustment is $\Delta p_{[dB]} = p_{1[dB]} - p_{0[dB]}$ and $p_{0[dB]}$ can be easily obtained from (1), the difficult on obtaining the CDF of $\Delta p_{[dB]}$ is to obtain the expression of $p_{1[dB]}$. Here, we need to consider three cases because the Rx may treat the direct and relay signals in different ways, depending on the value of the overall TDOA as well as the strength of the relay signal.

1) $\tau_K + \lambda_K \leq T_{\max}$ (Case A)

When the overall TDOA is less than or equals to $T_{\max}$ (called small delay), the Rx cannot distinguish the direct and relay signals. According to [21] [28], the average SNR at the Rx

can be expressed as

$$\bar{\gamma}_a \approx \frac{p_0 g_0 + G^2 p_0 g_1 g_2}{(G^2 g_2 + 1)\sigma^2} = \frac{p_0 g_e^a}{\sigma^2}, \tag{9}$$

where

$$g_e^a = \frac{g_0 + G^2 g_1 g_2}{G^2 g_2 + 1} \tag{10}$$

represents the *equivalent channel gain* (ECG) between the Tx and the Rx. Under CLPC, the transmission power of the Tx automatically changes from p_0 to

$$p_1^a = \bar{\gamma}_T \sigma^2 / g_e^a. \tag{11}$$

2) $\tau_K + \lambda_K > T_{\max}$

When the overall TDOA is larger than $T_{\max}$ (called large delay), the Rx treats the strong one as the desired signal and the weak one as the interference. Since either the direct signal from the Tx or the relay signal from the sensor can be the strong one, we have two situations:

a: Strong Direct Signal (Case B)

The Rx treats the direct signal as the desired signal if it can provide higher SINR than that the relay signal can provide. Conducting the similar derivation as in Case A, we can obtain the average SINR at the Rx, i.e.,

$$\bar{\gamma}_b \approx \frac{1}{2}\left(\frac{p_0 g_0}{G^2 p_0 g_1 g_2 + G^2 g_2 \sigma^2 + \sigma^2} + \frac{p_0 g_0}{\sigma^2}\right) = \frac{p_0 g_e^b}{\sigma^2}, \tag{12}$$

where the ECG is

$$g_e^b = \frac{\sigma^2 g_0}{2}\left(\frac{1}{G^2 p_0 g_1 g_2 + G^2 g_2 \sigma^2 + \sigma^2} + \frac{1}{\sigma^2}\right). \tag{13}$$

Under CLPC, the transmission power of the Tx automatically changes from p_0 to

$$p_1^b = \bar{\gamma}_T \sigma^2 / g_e^b. \tag{14}$$

b: Strong Relay Signal (Case C)

The Rx treats the relay signal as its desired signal if it can provide higher SINR than that the direct signal can provide. Again, conducting the similar derivation as in Case A, we can obtain the average SINR at the Rx, i.e.,

$$\bar{\gamma}_c \approx \frac{G^2 p_0 g_1 g_2}{p_0 g_0 + G^2 g_2 \sigma^2 + \sigma^2} = \frac{p_0 g_e^c}{\sigma^2}, \tag{15}$$

where the EGC is

$$g_e^c = \frac{G^2 g_1 g_2}{\frac{p_0 g_0}{\sigma^2} + G^2 g_2 + 1} = \frac{G^2 g_1 g_2}{\bar{\gamma}_T + G^2 g_2 + 1}. \tag{16}$$

Under CLPC, the transmission power of the Tx automatically changes from p_0 to

$$p_1^c = \bar{\gamma}_T \sigma^2 / g_e^c. \tag{17}$$

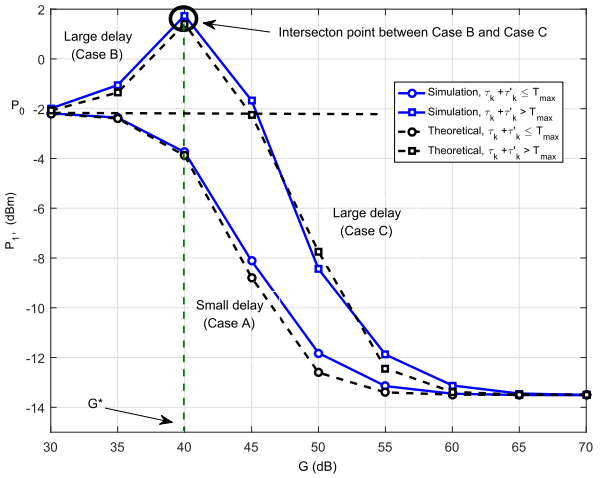

FIGURE 5. The Tx transmission power during the sensor's full-duplex AF relaying, where the amplitude gain is *G*.

3) DISCUSSION

We provide an example in Fig. 5 to show both simulation and theoretical results of the Tx transmission power, where the theoretical curves are obtained from (11), (14), and (17), respectively. The Tx, the Rx, and the sensor are located at (0, 0), (200, 0), and (130, 75) in meter. Other parameters are the same as Section V. In the figure, the small delay curves with the legend $\tau_k + \lambda_k \le T_{\max}$ have one segment, labeled as Case A. The large delay curves with the legend $\tau_k + \lambda_k > T_{\max}$ have two segments, labelled as Case B and Case C, respectively.

From the figure, we observe that the maximum gap between the simulation and theoretical curves is less than 1 dB. This indicates that the approximations in (9), (12), and (15) are valid. Furthermore, the small delay curves are always lower than the value p_0, which means that the relaying does not cause interference to the Rx. In contrast, when the amplitude gain is between 30 dB and 45 dB, the large delay curves are greater than the value p_0, which means that the relaying causes interference to the Rx. More importantly, we observe that the largest Tx transmission power appears at the intersection point between Case B and Case C. This allows us to do the worst case analysis to evaluate the interference, which will be discussed in the next subsection.

B. THE CDF OF THE TX POWER ADJUSTMENT

In this subsection, we derive the CDF expression of the Tx power adjustment, where the worst case is considered. As mentioned before, the worst case occurs at the intersection point between Case B and Case C in Fig. 5. At this point, the equality $g_b = g_c$ is satisfied, then the corresponding amplitude gain becomes

$$G^* = \sqrt{\frac{-V + \sqrt{V^2 + 4UW}}{2Ug_2}}, \tag{18}$$

where $U = 2\bar{\gamma}_S^2 + 2\rho^2\bar{\gamma}_S - \rho^2\bar{\gamma}_S\bar{\gamma}_T - \rho^4\bar{\gamma}_T$, $V = 2\bar{\gamma}_S - \bar{\gamma}_S\bar{\gamma}_T^2 - \rho^2\bar{\gamma}_T^2 - 3\rho^2\bar{\gamma}_T - \bar{\gamma}_S\bar{\gamma}_T$, and $W = 2(\bar{\gamma}_T^2 + \bar{\gamma}_T)$. This means that if the sensor chooses the amplitude gain G^* to conduct the relaying, it causes the strongest interference to the Rx[5].

If we make the following approximations, i.e., $U \approx 2\bar{\gamma}_S^2$, $V \approx -\bar{\gamma}_S\bar{\gamma}_T^2$, and $W \approx 2\bar{\gamma}_T^2$., we can simplify (18) to

$$G^* \approx \sqrt{\frac{\bar{\gamma}_T^2 + \bar{\gamma}_T\sqrt{\bar{\gamma}_T^2 + 16}}{4\bar{\gamma}_S g_2}}. \tag{19}$$

Let $\Lambda = \bar{\gamma}_T^2 + \bar{\gamma}_T\sqrt{\bar{\gamma}_T^2 + 16}$ and consider (16) and (19), we can obtain the ECG at the worst case as

$$g_e^* = \frac{1}{\frac{4p_0\bar{\gamma}_T}{\Lambda\sigma^2} + \frac{4p_0}{\Lambda\sigma^2} + \frac{1}{g_1}} \tag{20}$$

and the corresponding Tx transmission power becomes

$$p^* = \bar{\gamma}_T\sigma^2\left(\frac{4p_0\bar{\gamma}_T}{\Lambda\sigma^2} + \frac{4p_0}{\Lambda\sigma^2} + \frac{1}{g_1}\right). \tag{21}$$

Using dB unit, the above expression can be rewritten as

$$p^*_{[dB]} = \bar{\gamma}_{T[dB]} + \sigma^2_{[dB]} + 10\lg\left(\frac{4p_0\bar{\gamma}_T}{\Lambda\sigma^2} + \frac{4p_0}{\Lambda\sigma^2} + \frac{1}{g_1}\right). \tag{22}$$

We adopt the path loss model $g_{1_{[dB]}} = -128.1 - 37.6\lg(d)$ from [30], where d is the distance between the Tx and the sensor. Then, we have

$$\begin{aligned} F_{\Delta p_{[dB]}}(\Omega) &= \Pr\left\{\Delta p_{[dB]} < \Omega\right\} \\ &= \Pr\left\{\bar{\gamma}_{T[dB]} + \sigma^2_{[dB]} + 10\lg\left(\frac{4p_0\bar{\gamma}_T}{\Lambda\sigma^2} + \frac{4p_0}{\Lambda\sigma^2} + \frac{1}{g_1}\right)\right. \\ &\quad \left. - p_{0[dB]} < \Omega\right\} = \Pr\left\{d < 10^{-\frac{10\lg\left(\frac{1}{Z(\Omega)}\right)+128.1}{37.6}}\right\}, \end{aligned} \tag{23}$$

where

$$Z(\Omega) = 10^{\frac{\Omega + p_{0[dB]} - \bar{\gamma}_{T[dB]} - \sigma^2_{[dB]}}{10}} - \frac{4p_0\bar{\gamma}_T}{\Lambda\sigma^2} - \frac{4p_0}{\Lambda\sigma^2}. \tag{24}$$

Define $\rho = 10^{-\frac{10\lg\left(\frac{1}{Z(\Omega)}\right)+128.1}{37.6}}$ and based on Appendix A, we can obtain the close-form CDF expression of the Tx power adjustment as follows:

- When the Tx-Rx distance is small, i.e., $d_0 \le T_{\max}C/2$, we have

$$F_{\Delta p_{[dB]}}(\Omega) = \frac{\rho^2 - \zeta^2}{4c^2 - \zeta^2}, \tag{25}$$

  where $\zeta = 35$ m.
- When the Tx-Rx distance is large, i.e., $d_0 > T_{\max}C/2$, we have

$$F_{\Delta p_{[dB]}}(\Omega) = \begin{cases} \dfrac{\pi\rho^2 - \zeta^2}{S_1 - \pi\zeta^2}, & \rho \le \dfrac{T_{\max}C}{2}, \\ \dfrac{S_2 - \pi\zeta^2}{S_1 - \pi\zeta^2}, & \rho > \dfrac{T_{\max}C}{2}, \end{cases} \tag{26}$$

  where S_1 and S_2 are the areas of the whole Region I and a part of Region I, respectively, as in Appendix A.

[5]In fact, the localization sensor does not need to know the value of G^* since we only conduct the worse case analysis based on G^*.

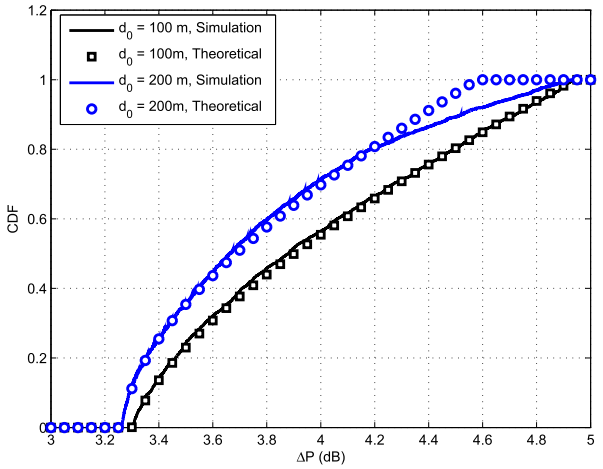

FIGURE 6. The CDF of the Tx power adjustment, i.e., $\Delta P = p_1 - p_0$, where p_0 and p_1 are the transmission powers of the Tx before and during the full-duplex AF relaying.

C. INTERFERENCE TO THE TX-RX LINK

In this subsection, we discuss the interference to the Tx-Rx link using Fig. 6, which shows the CDF curves of the Tx power adjustment. In particular, both simulation and theoretic results are provided. The parameter setting is the same as that in Section V. From the figure, we observe that the theoretic and simulation curves overlap very well in most situations. Therefore, the approximation in our derivation is valid. When we compare the curves with different Tx-Rx distances, we observe that the larger the Tx-Rx distance is, the larger the Tx power adjustment is, and the more interference it introduces. In addition, all curves approach 1 if the Tx-Rx link is able to tolerant $\Omega = 5$ dB power growth. This means that for $\Omega = 5$ dB, the sensors do not cause any interference to the Tx-Rx link.

V. SIMULATION RESULTS

In this section, we provide simulation results to demonstrate the performance of the proposed localization method. We assume that the interference threshold is $\Omega = 5$ dB, then the sensors do not cause interference to the Rx. For each simulation curve, it is averaged over $Q = 1000$ Monte Carlo trials. We choose the following set of parameters: the radius of the Rx coverage is 500 m, the maximum allowable TDOA is $T_{\max} = 10^{-6}$ s, the target SNR at the Rx is $\gamma_T = 10$ dB, the noise power is -114 dBm, the number of blocks is $N = 300$, and the number of sample in each block is $M = 200$.

In the wireless channels, the channel gain g_i (i = 0, 1, 2) is determined by both path loss and shadowing, i.e., $g_i = g_{p_i}(d)\cdot g_{s_i}$, where the path loss coefficient follows $g_{p_i[\mathrm{dB}]}(v) = -128.1 - 37.6\log_{10}(v)$, $v > 35$ m is the minimum distance between two nodes, and the shadowing coefficient $g_{s_i[\mathrm{dB}]}$ follows the log-normal distribution with mean zero and the standard deviation $\sigma'_{[\mathrm{dB}]}$.

For performance evaluation, we consider the *root-mean-square-error* (RMSE), which is defined as RMSE $= \sqrt{\mathbb{E}\left[(\hat{x}-x)^2+(\hat{y}-y)^2\right]}$, where (x, y) is the true location of the Rx, and $(\hat{x}, \hat{y})$ is the estimated location of the Rx. We also consider the successful estimation probability ξ, which is defined as $\xi = q/Q$, where Q is the number of Monte Carlo trials, and q is the number of positive estimation values.

In the following, we first choose the values of the amplitude gain, the threshold, the number of sensors, and the increasing step of the added time delay, where both localization RMSE and successful estimation probability are considered. Then, we provide the performance of the proposed algorithm under the shadowing, where the imperfect *self-interference suppression* (SIS) is also considered. For the imperfect SIS, we raise the noise floor at each sensor by 2 dB according to [21], [31].

A. PARAMETER SELECTION

1) AMPLITUDE GAINS AND THRESHOLD

Fig. 7 and 8 provide the performance of the Rx localization under different amplitude gains, where different thresholds in TDOA estimation are considered. Here, the increasing step of the added time delay is $\epsilon = 10^{-9}$ s and the number of sensors is $K = 9$. From Fig. 7, all RMSE curves have an "U" shape between 45 dB $< G <$ 60 dB. This is reasonable because when the sensors conduct the relaying, the small amplitude gain G cannot trigger the CLPC effectively, while the large amplitude gain G saturates the CLPC. As a result, the minimum RMSE is obtained at $G = 50$ dB. Meanwhile, the maximum successful estimation probability can be roughly obtained at $G = 50$ dB under our system settings. We notice that the RMSE curves are not stable for $G < 45$ dB and $G > 60$ dB. This is because the successful estimation probability is very low in these regions. In addition, when we further compare the curves with different thresholds η, the best performance can be obtained at $\eta_{[dB]} = 2$ dB, where the RMSE is below 2 m and the successful estimation probability is about 99%.

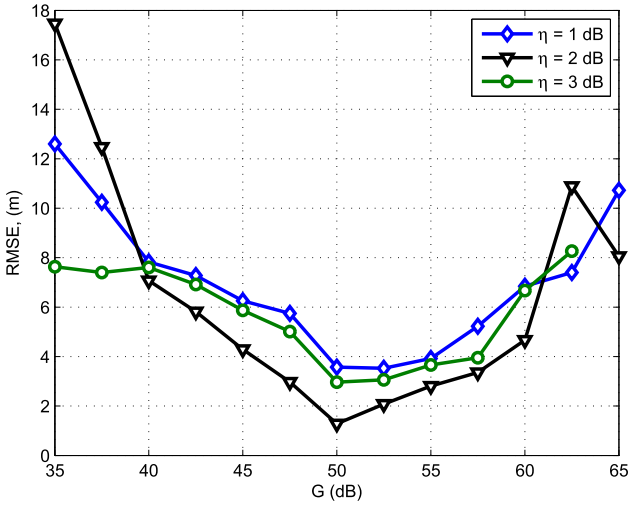

FIGURE 7. The RMSE v.s. the amplitude gain *G*.

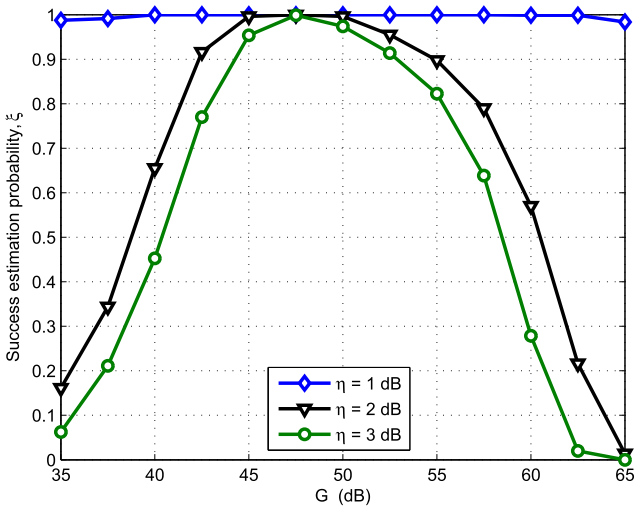

FIGURE 8. The successful estimation probability v.s. the amplitude gain *G*.

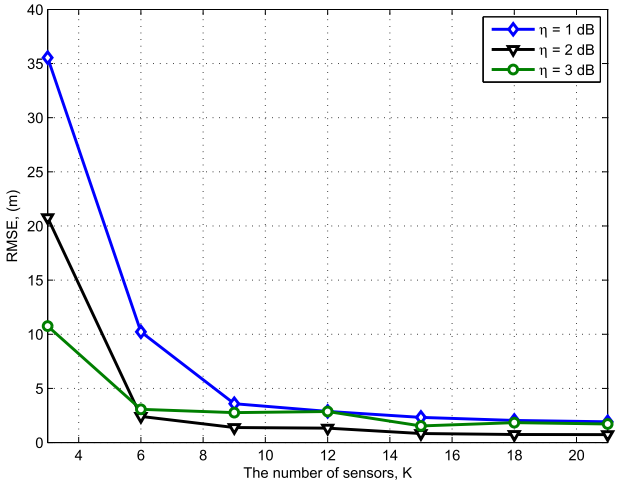

FIGURE 9. The RMSE v.s. the number of sensors.

2) NUMBER OF SENSORS

Fig. 9 and 10 show the performance of the Rx localization under different number of sensors. Here, the increasing step of the added time delay is $\epsilon = 10^{-9}$ s and the amplitude gain is $G = 50$ dB. From the figures, as the number of sensors increases from 3 to 9, the RMSE curves decrease dramatically. The corresponding successful estimation probability increases dramatically. When the number of sensors keeps on growing and becomes large than 9, all curves become constant. Thus, we choose $K = 9$ sensors for the rest of the simulation.

3) INCREASING STEPS OF THE ADDED TIME DELAY (I.E., RESOLUTION OF CONTROLLED TIME DELAY)

Fig. 11 and 12 demonstrate the performance of the Rx localization under different increasing steps of the added time

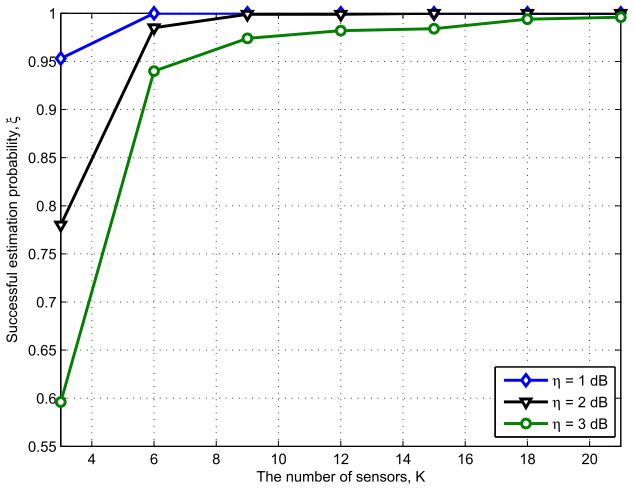

FIGURE 10. The successful estimation probability v.s. the number of sensors.

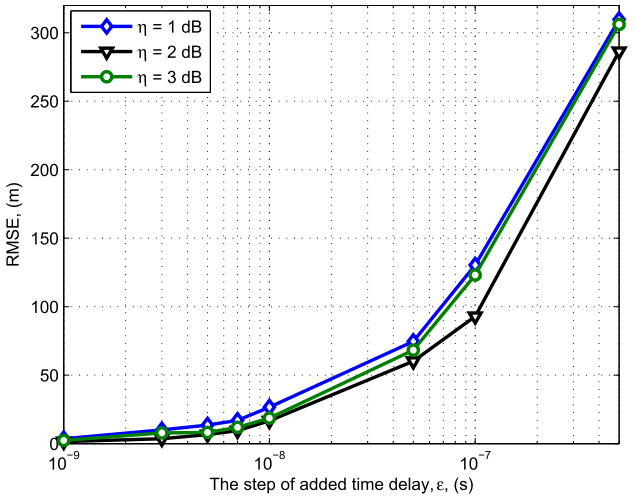

FIGURE 11. The RMSE v.s. the increasing step of the added time delay.

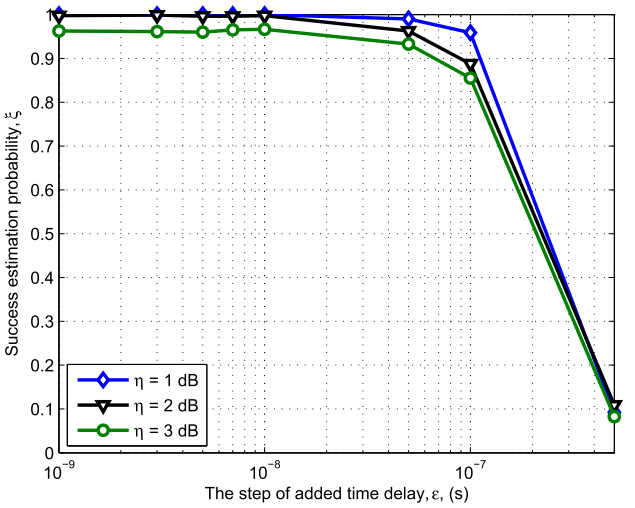

FIGURE 12. The success estimation probability v.s. the increasing step of the added time delay.

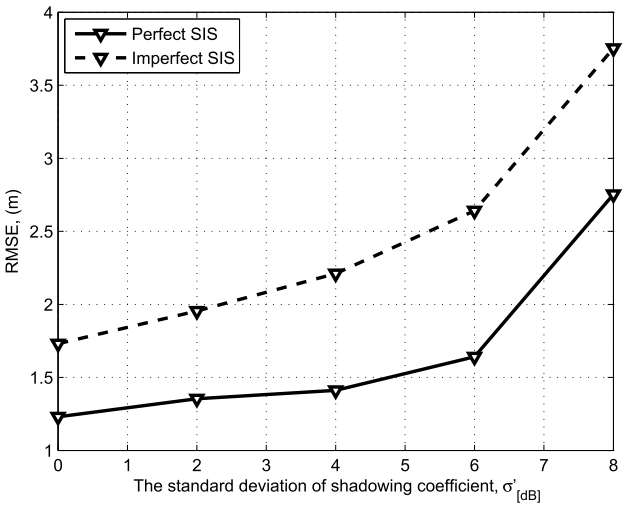

FIGURE 13. The RMSE v.s. the shadowing coefficient.

delay[6]. Here, the amplitude gain is $G = 50$ dB and the number of sensors is $K = 9$. From the figures, as the increasing step grows, the RMSE curves increase while the successful estimation probability curves decrease. This is reasonable because the large step leads to the large estimation error in TDOA estimation. This further results in large RMSE in Rx localization. In particular, the RMSE is about 20 m and 3 m for $\epsilon = 10^{-8}$ s and $\epsilon = 10^{-9}$, respectively. The corresponding successful estimation probabilities are identical and they are equal to about 99% for the threshold at $\eta = 2$ dB.

[6]In practice, there are many ways to control the added time delay at 10^{-9} s level, e.g., Dallas Semiconductor DS1020 Chip is able to adjust the time delay as low as 0.15×10^{-9} s per step. We notice that when conducting the full-duplex relaying, the circuit of the localization sensor may inevitably introduce a time delay, from several nanoseconds to hundred nanoseconds [32]. But, this does not affect the nano-level time delay adjustment because the circuit delay is usually a constant and can be known to the sensor. During the localization, the circuit delay can be canceled directly. Thus, we do not consider the circuit delay in this paper, which facilitates the development of our idea.

To reach the meter-level localization performance, we choose $\epsilon = 10^{-9}$ s in the rest of the simulation.

B. LOCALIZATION PERFORMANCE UNDER SHADOWING AND IMPERFECT SIS

Fig. 13 shows the RMSE performance under different standard deviation of the shadowing, where the imperfect SIS is also considered. We assume that the amplitude gain is $G = 50$ dB, the number of sensors is $K = 9$, the increasing step of the added time delay is $\epsilon = 1 \times 10^{-9}$ s, and the threshold in TDOA estimation is $\eta = 2$ dB. In particular, the Tx-Rx distance is $d_0 = 200$ m. Here, we do not provide the successful probability performance since it approaches to 1 in the above settings. In the following, we first consider the perfect SIS. From the figure, as the standard deviation of the shadowing grows from 0 dB to 8 dB, the RMSE curve slightly increases. This is reasonable since the proposed method is

based TDOA estimation, which is not sensitive to the shadowing. In addition, we consider the imperfect SIS, it only causes minor performance loss. This is reasonable since the proposed method is mainly based on the power adjustment of the Tx. Before and after adding a time delay, the residual self-interference is almost the same. Then the residual self-interference can be canceled during the detection. Therefore, for a typical scenario with the shadowing at $\sigma' = 6$ dB, the proposed method can achieve the RMSE below 3 m.

VI. CONCLUSIONS AND FURTHER WORK

In this paper, we proposed a relay-assisted method to localize a noncooperative receiver without knowing the spectrum that the receiver uses for backward transmission. In our method, the localization sensors alternatively conduct the full-duplex AF relaying to create an artificial relay path for the receiver. By estimating the TDOA using the proposed delay-relay algorithm, the localization sensors are able to calculate the location of the receiver from triangulation. To validate the feasibility of the proposed localization method, we further analyzed the power adjustment of the transmitter, which indicates the interference to the communication link between the transmitter and receiver. From simulation results, the proposed localization method can meet the interference constraint and effectively localize the noncooperative Rx.

While this paper focuses on introducing the new localization approach and demonstrating its feasibility, many extensions can be treated as the future works. For example, new localization algorithms may need to be developed for other mechanisms such as AMC and ARQ in link adaption; some imperfections need to be further considered, e.g., the time delay and the quantization of the link adaption feedback, the signal processing delay of the circuits; and the extensions to multi-path channels and multiple antenna systems are other research directions.

APPENDIX

VII. DERIVATION OF THE CDF EXPRESSION OF $\delta P_{[DB]}$

In this appendix, we first provide the model that is used in our derivation. Then, we provide the details to obtain the closed-form CDF expression of $\Delta p_{[dB]}$.

We adopt the four region geographical model as in [21], which is shown Fig. 14. In the figure, the whole coverage of the Tx can be divided into four regions by the dashed circle and solid ellipse, i.e., Regions I, II, III, and IV. We denote I_c and I_e as the regions inside the dashed circle and solid ellipse, respectively. We further denote $\overline{I_c}$ and $\overline{I_e}$ as the regions outside the dashed circle and solid ellipse, respectively. Then, the four regions can be expressed as (1) Region I $= I_c \cap I_e$; (2) Region II $= \overline{I_c} \cap I_e$; (3) Region III $= I_c \cap \overline{I_e}$; (4) Region IV $= \overline{I_c} \cap \overline{I_e}$.

In addition, for the dashed circle, the center is the Tx and the radius is the Tx-Rx distance d_0. For the solid ellipse, the two foci are the Tx and Rx. The boundary of the ellipse is determined by the maximum allowable TDOA $T_{\max}$. If a sensor is located at any point on the ellipse, the length of the relay paths is equal to a certain value and the corresponding TDOA

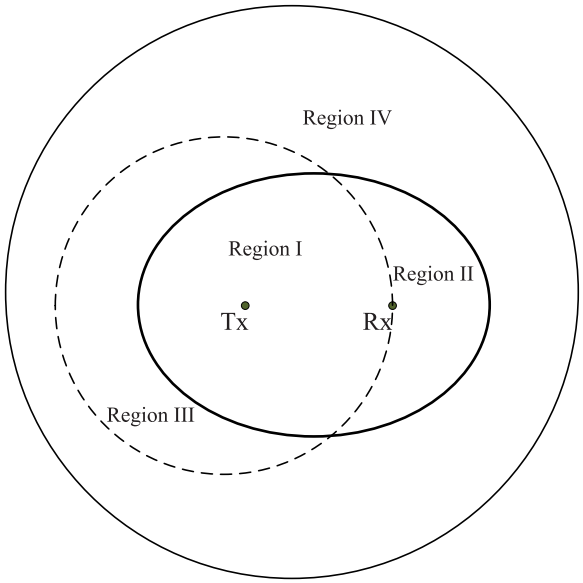

FIGURE 14. Four region geographical model.

at the Rx is $T_{\max}$. Then, the difference of the propagation distances between the direct and relay paths becomes $T_{\max} \cdot C$, where C is a constant. Based on ellipse equations, the parameters of the ellipse can be obtained, i.e., the semi-focal length is $c = d_0/2$, the semi-major axis is $a = T_{\max}C/2 + c$, and semi-minor axis is $b = \sqrt{a^2 - c^2}$, where d_0 is the Tx-Rx distance.

Next, we discuss how to obtain the CDF expression of $\Delta p_{[dB]}$. Specifically, the expression (23) indicates that value of the CDF is equal to the probability that sensor fills into a disk region with the center at the Tx and the radius at ρ. If the sensor is uniformly distributed inside Region I, which can be realized by the selection method in [21], then calculating the value of the CDF is equivalent to calculating the ratio of the two areas: one is the common area of the disk region and the Region I, and the other is the whole area of the Region I. In the following, we consider different cases to obtain the expressions of the two areas. After that we can obtain the expressions of the required CDF expression.

- Case 1:
  If the Tx-Rx distance is small, i.e., $d_0 \leq T_{\max}C/2$, the whole area of the dashed circle is inside the ellipse, which is shown in Fig. 15. Then, the coverage of the Tx has three regions, i.e., Regions I, II, and IV. In this case, the whole disk region is inside Region I. We can obtain the CDF expression as follows

$$F_{\Delta p_{[dB]}}(\Omega) = \Pr\{d < \rho\} = \frac{\rho^2 - \zeta^2}{4c^2 - \zeta^2}. \quad (27)$$

- Case 2:
  If the Tx-Rx distance is large, i.e., $d_0 > T_{\max}C/2$, only a part of the dashed circle is inside the ellipse. Then, the coverage of the Tx has four regions, i.e., Regions I, II, III, and IV. In this case, depending on the value of the radius ρ, we can further obtain two sub-cases as follows:

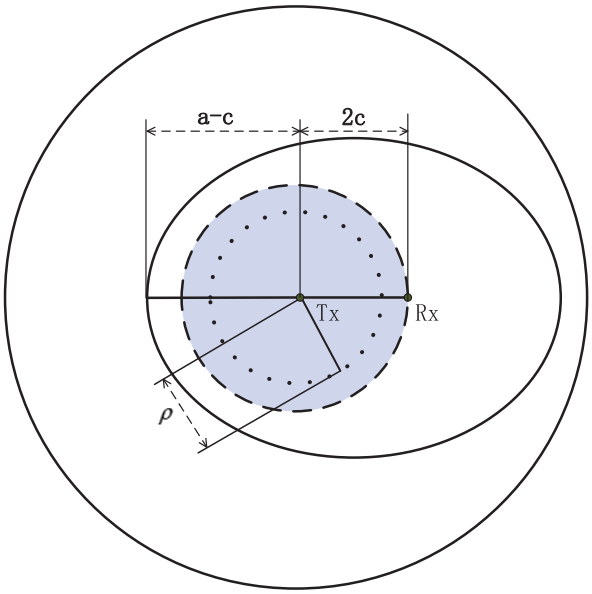

FIGURE 15. Geographical region model for the CDF derivation in Case 1.

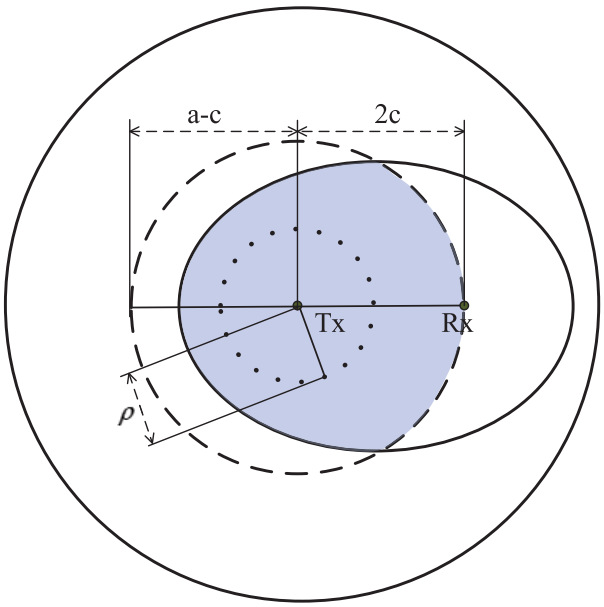

FIGURE 16. Geographical region model for the CDF derivation in Case 2-a.

- Case 2-a: If $\rho \leq T_{\max}C/2$, the whole region of the disk with the radius ρ is inside Region I, which is shown in Fig. 16. Then, we can obtain the CDF expression as follows

$$F_{\Delta p_{[dB]}}(\Omega) = \Pr\{d < \rho\} = \frac{\pi\rho^2 - \pi\zeta^2}{S_1 - \pi\zeta^2}, \quad (28)$$

  where S_1 is the area of the Region I and will be obtained at the end of this appendix.
- Case 2-b: If $\rho > T_{\max}C/2$, only a part of the disk with the radius ρ is inside Region I, which is shown in Fig. 17. Then, we can obtain the CDF expression as follows

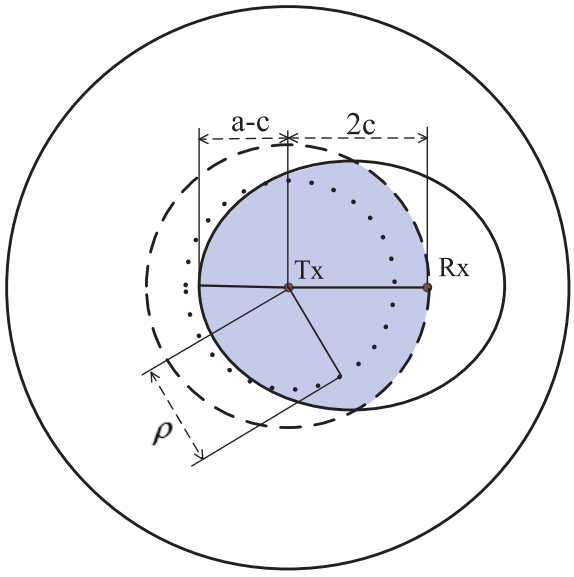

FIGURE 17. Geographical region model for the CDF derivation in Case 2-b.

$$F_{\Delta p_{[dB]}}(\Omega) = \Pr\{d_1' < \rho\} = \frac{S_2 - \pi\zeta^2}{S_1 - \pi\zeta^2}, \quad (29)$$

  where S_s is the common area of the disk and Region I.

In rest of this appendix, we derive the expressions of S_1 and S_2 in (28) and (29). As shown in Fig. 16, we first obtain the two intersection points (x', y') between the ellipse and the dashed circle by solving the following equations

$$x'^2 + y'^2 = (2c)^2, \quad (30)$$

$$\frac{(x'-c)^2}{a^2} + \frac{y'^2}{b^2} = 1. \quad (31)$$

Then, we have

$$\begin{cases} x' = \dfrac{-b^2 \pm 2ac}{c}, \\ y' = \pm\dfrac{b\sqrt{4ac - (4c^2 + b^2)}}{c}. \end{cases} \quad (32)$$

Since the left endpoint of the ellipse is $(c-a, 0)$ and $a - c < 2c < a + c$, we can obtain the following inequality

$$(c-a) - \frac{-b^2 - 2ac}{c} = \frac{a(a-c) + 2ac}{c} > 0. \quad (33)$$

It indicates that the solution $(\frac{-b^2-2ac}{c}, \frac{\pm b}{c\sqrt{4ac-(4c^2+b^2)}})$ can be ruled out. As a result, the two intersection points become $((-b^2 + 2ac)/c, \pm b/c\sqrt{4ac - (4c^2 + b^2)})$.

By calculating the integration, we can obtain the expression of S_1 as follows

$$\begin{aligned} S_1 &= 2\int_{c-a}^{\frac{-b^2+2ac}{c}} y' dx' + \Psi \\ &= 2\int_{\pi}^{\theta_1} b\sin\alpha(-a\sin\omega)d\omega + \Psi \end{aligned}$$

$$= 2ab\int_{\theta_1}^{\pi}\sin^2\omega d\omega + \Psi$$
$$= ab(\pi-\theta_1) + \frac{1}{2}ab\sin(2\theta_1) + \Psi, \tag{34}$$

where $\theta_1 = \arccos((2c-a)/c)$ and

$$\Psi = \begin{cases} 4c^2\arctan(\dfrac{|y'|}{x'_0}) - |x'y'|, & x' > 0, \\ 4c^2[\pi + \arctan(\dfrac{|y'|}{x'})] - |x'y'|, & x' < 0, \\ \dfrac{4\pi c^2}{2}, & x' = 0. \end{cases} \tag{35}$$

Similarly, we can obtain the expression of S_2 as follows

$$S_2 = ab(\pi-\theta_2) + \frac{1}{2}ab\sin(2\theta_2) + \Psi', \tag{36}$$

where $\theta_2 = \arccos((\rho-a)/c)$ and

$$\Psi' = \begin{cases} \rho^2\arctan(\dfrac{b\sqrt{2a\rho-\rho^2-b^2}}{a\rho-b^2}) \\ \quad - \dfrac{b(a\rho-b^2)\sqrt{2a\rho-\rho^2-b^2}}{c^2}, \\ \qquad\qquad a\rho - b^2 > 0, \\ \rho^2[\pi + \arctan(\dfrac{b\sqrt{2a\rho-\rho^2-b^2}}{a\rho-b^2})] \\ -\dfrac{b(a\rho-b^2)\sqrt{2a\rho-\rho^2-b^2}}{c^2}, \quad a\rho - b^2 < 0, \\ \dfrac{\pi\rho^2}{2}, \qquad\qquad a\rho - b^2 = 0. \end{cases} \tag{37}$$

ACKNOWLEDGMENT

This paper was presented at INFOCOM 2016 and ICC 2016.

REFERENCES

[1] M. Z. Win, Y. Shen, and W. Dai, "A theoretical foundation of network localization and navigation," *Proc. IEEE*, vol. 106, no. 7, pp. 1136–1165, Jul. 2018.

[2] G. Han, J. Jiang, C. Zhang, T. Q. Duong, M. Guizani, and G. Karagiannidis, "A survey on mobile anchor node assisted localization in wireless sensor networks," *IEEE Commun. Surveys Tuts.*, vol. 18, no. 3, pp. 2220–2243, 3rd Quart., 2016.

[3] K. Witrisal *et al.*, "High-accuracy localization for assisted living: 5G systems will turn multipath channels from foe to friend," *IEEE Signal Process. Mag.*, vol. 33, no. 2, pp. 59–70, Mar. 2016.

[4] S. Bartoletti, W. Dai, A. Conti, and M. Z. Win, "A mathematical model for wideband ranging," *IEEE J. Sel. Topics Signal Process.*, vol. 9, no. 2, pp. 216–228, Mar. 2015.

[5] A. Conti, M. Guerra, D. Dardari, N. Decarli, and M. Z. Win, "Network experimentation for cooperative localization," *IEEE J. Sel. Areas Commun.*,vol. 30, no. 2, pp. 467–475, Feb. 2012.

[6] I. Guvenc and C.-C. Chong, "A survey on TOA based wireless localization and NLOS mitigation techniques," *IEEE Commun. Surveys Tuts.*, vol. 11, no. 3, pp. 107–124, 3rd Quart., 2009.

[7] H. Wymeersch, J. Lien, and M. Z. Win, "Cooperative localization in wireless networks," *Proc. IEEE*, vol. 97, no. 2, pp. 427–450, Feb. 2009.

[8] D. Dardari, A. Conti, U. Ferner, A. Giorgetti, and M. Z. Win, "Ranging with ultrawide bandwidth signals in multipath environments," *Proc. IEEE*, vol. 97, no. 2, pp. 404–426, Feb. 2009.

[9] Y. Shen, W. Dai, and M. Z. Win, "Power optimization for network localization," *IEEE/ACM Trans. Netw.*, vol. 22, no. 4, pp. 1337–1350, Aug. 2014.

[10] N. Salman, M. Ghogho, and A. H. Kemp, "On the joint estimation of the RSS-based location and path-loss exponent," *IEEE Wireless Commun. Lett.*, vol. 1, no. 1, pp. 34–37, Feb. 2012.

[11] A. Jafari *et al.*, "NLOS influence on 60 GHz indoor localization based on a new TDOA extraction approach," in *Proc. IEEE Microw. Conf. (EuMC)*, Oct. 2013, pp. 330–333.

[12] C. Steiner and A. Wittneben, "Efficient training phase for ultrawideband-based location fingerprinting systems," *IEEE Trans. Commun.*, vol. 59, no. 12, pp. 6021–6032, Dec. 2011.

[13] Z. Wang and W. Zhang, *Opportunistic Spectrum Sharing in Cognitive Radio Networks*. Berlin, Germany: Springer, 2015.

[14] G. Zhao, W. Zhang, and S. Li, *Advanced Sensing Techniques for Cognitive Radio*. Berlin, Germany: Springer, 2016.

[15] P. E. Biglieri, P. A. J. Goldsmith, L. J. Greenstein, N. B. Mandayam, and H. V. Poor, *Principles of Cognitive Radio*. Cambridge, U.K.: Cambridge Univ. Press, 2012.

[16] G. Zhao, B. Huang, L. Li, and Z. Chen, "Estimate the primary-link SNR using full-duplex relay for underlay spectrum sharing," *IEEE Signal Process. Lett.*, vol. 23, no. 4, pp. 429–433, Apr. 2016.

[17] G. Zhao, G. Li, and C. Yang, "Proactive detection of spectrum opportunities in primary systems with power control," *IEEE Trans. Wireless Commun.*, vol. 8, no. 9, pp. 4815–4823, Sep. 2009.

[18] R. Zhang, "On active learning and supervised transmission of spectrum sharing based cognitive radios by exploiting hidden primary radio feedback," *IEEE Trans. Commun.*, vol. 58, no. 10, pp. 2960–2970, Oct. 2010.

[19] H. A. Suraweera, P. J. Smith, and M. Shafi, "Capacity limits and performance analysis of cognitive radio with imperfect channel knowledge," *IEEE Trans. Veh. Technol.*, vol. 59, no. 4, pp. 1811–1822, May 2010.

[20] F. Yuan, G. P. Villardi, F. Kojima, and H. Yano, "Channel direction information probing for multi-antenna cognitive radio system," *EURASIP J. Adv. Signal Process.*, vol. 2015, no. 1, pp. 1–13, Dec. 2015.

[21] G. Zhao, B. Huang, L. Li, and X. Zhou, "Relay-assisted cross-channel gain estimation for spectrum sharing," *IEEE Trans. Commun.*, vol. 64, no. 3, pp. 973–986, Mar. 2016.

[22] B. Huang, G. Zhao, L. Li, X. Zhou, and Z. Chen, "Non-cooperative cross-channel gain estimation using full-duplex amplify-and-forward relaying in cognitive radio networks," in *Proc. IEEE Int. Conf. Acoust., Speech, Signal Process. (ICASSP)*, Mar. 2016, pp. 3636–3640.

[23] G. Zhao, B. Chang, Z. Chen, L. Li, and J. Liang, "Third-party receiver positioning in wireless sensor networks," in *Proc. IEEE Conf. Comput. Commun. Workshops*, Apr. 2016, pp. 754–759.

[24] B. Chang, G. Zhao, Z. Chen, and L. Li, "Positioning third-party receiver via TDOA estimation in frequency duplex division systems," in *Proc. IEEE Int. Conf. Commun. (ICC)*, May 2016, pp. 1–6.

[25] Z. K. M. Ho and E. A. Jorswieck, "Instantaneous relaying: Optimal strategies and interference neutralization," *IEEE Trans. Signal Process.*, vol. 60, no. 12, pp. 6655–6668, Dec. 2012.

[26] Y. Y. Kang and J. H. Cho, "Capacity of MIMO wireless channel with full-duplex amplify-and-forward relay," in *Proc. 20th IEEE Int. Symp. Pers., Indoor Mobile Radio Commun. (PIMRC)*, Sep. 2009, pp. 117–121.

[27] L. Rodriguez, N. Tran, and T. Le-Ngoc, *Amplify-and-Forward Relaying in Wireless Communications*. Berlin, Germany: Springer, 2015.

[28] T. Riihonen and R. Wichman, "Power allocation for a single-frequency fixed-gain relay network," in *Proc. IEEE 18th Int. Symp. Pers., Indoor Mobile Radio Commun. (PIMRC)*, Sep. 2007, pp. 1–5.

[29] B. Chang, Z. Guo, G. Zhao, Z. Chen, and L. Li, "Positioning receiver using full-duplex amplify-and-forward relay," in *Proc. IEEE Global Telecommun. Conf. (GLOBECOM)*, Dec. 2015, pp. 1–6.

[30] *Physical layer aspect for evolved Universal Terrestrial Radio Access (UTRA) (Release 7)*, document 3GPP TR 25.814, May 2006.

[31] Y. Liao, L. Song, Z. Han, and Y. Li, "Full duplex cognitive radio: A new design paradigm for enhancing spectrum usage," *IEEE Commun. Mag.*, vol. 53, no. 5, pp. 138–145, May 2015.

[32] D. Bharadia and S. Katti, "FastForward: Fast and constructive full duplex relays," in *Proc. ACM SIGCOMM.*, Aug. 2014, pp. 199–210.

CHUANXUE JIN received the M.S. degree from the National Key Laboratory on Communications, University of Electronic Science and Technology of China (UESTC), in 2006. He is currently a Lecturer with UESTC. His research interests include hardware design for wireless communication systems, such as filter bank multicarrier systems, wireless positioning, and cognitive radio networks.

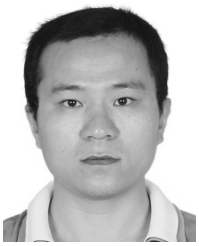

BO CHANG received the bachelor's degree in communication engineering from the University of Electronic Science and Technology of China (UESTC), Chengdu, China, in 2013, where he is currently pursuing the Ph.D. degree with the National Key Laboratory of Science and Technology on Communications. His research interests include cognitive radio, wireless localization, and communication-control co-design.

GUODONG (PHILIP) ZHAO (SM'16) received the B.E. degree from Xidian University, Xi'an, China, in 2005, and the Ph.D. degree from Beihang University, Beijing, China, in 2011. From 2011 to 2018, he was an Associate Professor with the University of Electronic Science and Technology of China, China. From 2012 to 2013, he visited The Hong Kong University of Science and Technology, Hong Kong. In 2016, he visited Lehigh University, Bethlehem, PA, USA. In 2018, he joined the University of Glasgow, U.K., as a Lecturer (Assistant Professor). He has authored over 50 papers in IEEE journals and conferences. His current research interests are within the areas of wireless communications and control. He received the Best Paper Award from the IEEE Global Telecommunication Conference in 2012 and the Best Ph.D. Thesis Award from Beihang University in 2012. He has served as a TPC for many international conferences, including ICC and VTC. He also served as a Reviewer for many IEEE Transactions, including the IEEE TRANSACTIONS ON SIGNAL PROCESSING and the *IEEE Journal on Selected Areas in Communications*.

ZHI CHEN (SM'16) received the B. Eng, M. Eng., and Ph.D. degrees in electrical engineering from the University of Electronic Science and Technology of China (UESTC), in 1997, 2000, and 2006, respectively. In 2006, he joined the National Key Laboratory of Science and Technology on Communications, UESTC, where he has been a Professor since 2013. He was a Visiting Scholar with the University of California at Riverside, Riverside, CA, USA, from 2010 to 2011. His current research interests include 5G mobile communications, tactile internet, and terahertz communication. He has served as a Reviewer for various international journals and conferences, including the IEEE TRANSACTIONS ON VEHICULAR TECHNOLOGY and the IEEE TRANSACTIONS ON SIGNAL PROCESSING.

YUAN SHEN (S'05–M'14) received the B.E. degree (Hons.) in electronic engineering from Tsinghua University, Beijing, China, in 2005, and the S.M. and Ph.D. degrees in electrical engineering and computer science from the Massachusetts Institute of Technology (MIT), Cambridge, MA, USA, in 2008 and 2014, respectively. He was a Research Assistant and then a Post-Doctoral Associate with the Wireless Information and Network Sciences Laboratory, MIT, from 2005 to 2014. He was with the Hewlett-Packard Labs in 2009 and the Corporate R&D, Qualcomm Inc., in 2008. He is currently an Associate Professor with the Department of Electronic Engineering, Tsinghua University. His research interests include statistical inference, network science, communication theory, information theory, and optimization. His current research focuses on network localization and navigation, inference techniques, resource allocation, and intrinsic wireless secrecy.